S. Afr. J. Chem., 2015, **68**, 226–235,
<http://journals.sabinet.co.za/sajchem/>.

Adsorption of Mercury(II) onto Activated Carbons derived from *Theobroma cacao* Pod Husk

Charles M. Kede[a,b], Peter P. Ndibewu[a,*], Makonga M. Kalumba[a], Nikolay A. Panichev[a], Horace M. Ngomo[c] and Joseph M. Ketcha[c]

[a]*Department of Chemistry, Tshwane University of Technology, P.O. Box 56208, Arcadia, Pretoria, 0007 South Africa.*

[b]*Department of Chemistry, Faculty of Science, University of Douala, P.O. Box 24175, Douala, Cameroon.*

[c]*Department of Chemistry, Faculty of Science, University of Yaoundé I, P.O. Box 812, Yaoundé, Cameroon.*

Received 3 September 2013, revised 18 April 2015, accepted 7 August 2015.

ABSTRACT

Activated carbon prepared from *Theobroma cacao* pod husk was used as a low-cost biosorbent for the removal of mercury(II) from aqueous solutions. The influence of pH and contact time on the adsorption was investigated by conducting a series of batch adsorption experiments. The equilibrium data were fitted to the Langmuir and Freundlich isotherm models. The Langmuir isotherm was found to best describe the experimental data. The amount adsorbed increased with increasing temperature. The maximum adsorption capacity of mercury was found to be 10^5 ng g^{-1} for an initial mercury concentration of 100 ppb. The kinetics of adsorption were modelled by means of the Lagergren-first-order and pseudo-second-order models. The pseudo-second-order model was found to explain the adsorption kinetics most effectively. It was also found that pore diffusion played an important role in the adsorption, and intra-particle diffusion was the rate-limiting step during the first 30 min. A FTIR study revealed that the carbonyl and sulfur functional groups present on the surface of the adsorbing material were involved in chemical interaction with mercury(II).

KEYWORDS

Mercury, thermal desorption, adsorption, activated carbon, *Theobroma cacao*, pod husk.

1. Introduction

Mercury (Hg) is one of the most harmful pollutants and it has become widespread in the environment mainly as a result of anthropogenic activities.[1–2] Mercury has no beneficial biological function and its presence in living organisms is associated with cancer, birth defects and other undesirable outcomes.[3] Mercury enters the human body mainly through sea food, drinking water and inhalation of polluted air.[4] Therefore, according to the United States Environmental Protection Agency (USEPA),[5] the tolerance limit for Hg^{2+} for drinking water is 1 μg L^{-1}. Hg^{2+} causes damage to the central nervous system and chromosomes, impairment of pulmonary function and kidneys, chest pain and dyspnoea.[6] Methylmercury (often written as methyl mercury) is an organometallic cation with the formula CH_3Hg^+ and is a serious bioaccumulative environmental toxicant.[7] The harmful effects of methylmercury include the contamination of fish,[7] an important source of protein around the world, especially for growing children. Hence, it is essential to remove Hg^{2+} from aqueous solution before its transport and cycling into the environment.

Conventional methods for removing Hg^{2+} from aqueous solutions include sulfide precipitation, ion exchange, alum and iron coagulation, adsorption on activated carbons and reverse osmosis.[8] However, Hg^{2+} removal costs for most of these methods are still very high. This has led to the intensification of research focussed on new materials and technologies that will provide for an effective and economic removal of Hg^{2+} from aqueous solutions. Recent developments have centred on the investigation of non-conventional adsorbents like bentonite,[9] modified forms of palm shell,[10] and natural and aluminium pillared clays[11] reported to be used with success to some extent for the removal of Hg^{2+} from aqueous solutions including waste Fe(III)/Cr(III) hydroxide.

Besides the economic implications, the use of agricultural by-products has many environmental advantages.[12] In the cocoa-producing regions of the world (e.g. Cameroon, the Ivory Coast and Ghana in Africa and Brazil in the Amazon) agricultural wastes such as *Theobroma cocoa* pod husk are often disposed of under unsuitable conditions. These then rot, generating bad smells (unhygienic) with considerable negative impacts on the landscape or provide favourable environments for microorganisms to flourish which eventually find their way into drinking water streams. Consequently, the use of *Theobroma cocoa* pod husk for the purpose of removing Hg^{2+} from aqueous solutions presents multiple advantages from an environmental point of view. Firstly, since it is disposed of as a waste, its use would add value to an agricultural by-product. Secondly, the importance of effective and economic removal of Hg^{2+} cannot be overemphasized here as it is a global problem. Thirdly, and finally, *Theobroma cocoa* pod husk may be considered as a renewable resource because it can be replenished continuously, while the cocoa beans would continue to be traded as an important cash crop in many developing countries.

Cocoa pod husk represents between 70 and 75 % of the whole mass of the cocoa fruit, i.e. 700 to 750 kg of waste can be generated from a ton of cocoa fruit. Nevertheless, various techniques have been developed as alternative methods of disposal while creating valuable products, e.g. food antioxidants,[13] dietary fibres,[14] and animal feed.[15] Cocoa pod husk possesses suitable characteristics making it a good precursor for the preparation of activated carbons owing to its cellulosic and hemicellulosic content.[16]

We reported from our preliminary findings that carbonized

* To whom correspondence should be addressed. E-mail chacdw@upe.ac.za

ISSN 0379-4350 Online / ©2015 South African Chemical Institute / http://saci.co.za/journal
DOI: http://dx.doi.org/10.17159/0379-4350/2015/v68a31

Theobroma cacao pod husk is effective for the treatment of dye in wastewater and the removal of As, Cd, Cr, Hg and Ni.[17] Other authors have also reported the successful removal of organics, including pesticides from aqueous solutions.[18] The objective of this study was to investigate the feasibility of using carbonized *Theobroma cacao* pod husk for the removal of Hg^{2+} from water by adsorption.

2. Experimental

2.1. Instrumentation

Mercury measurements from water samples were carried out after adsorption on the sorbent with a Model RA–915$^+$ Zeeman mercury analyzer (Lumex, St. Petersburg, Russia) fitted with a PYRO–915 attachment. The working principal of the instrument is based on the thermal desorption of Hg from samples placed in two-stage pyrolysis tubes heated to 750 and 800 °C. When a known amount of sample is placed in the first preheated tube, Hg vapour, together with smoke formed after combustion of the organic materials in the matrix, are transported to the second tube with the analytical cell preheated to 800 °C. A multi-path analytical cell with a total optical length of 0.4 m allows detection of Hg (in pg) because background absorption is eliminated by the high-frequency Zeeman correction system. The concentration of Hg in the sample is determined from the integrated analytical signal, by using the built-in calibration curve, plotted with different certified reference materials (CRMs). The PYRO–915 attachment enhances Hg determination in samples with complex matrices, such as soils, sediments, oil products and foodstuff, by using the pyrolysis technique without sample pretreatment.[19,20,21–22] Real-time measurements are made with visualization of the process on a computer display. With no chemical sample pretreatment and without addition of chemical modifiers, the risk of contamination is minimized.

2.2. Reagents and Reference Materials

All the chemicals used were of analytical reagent grade. Deionized doubly distilled (DDD) water was used throughout the experimental studies. Mercury standard solutions (10 mg L^{-1}, Atomic Spectroscopy Standard, PerkinElmer, Inc, USA) were prepared by progressive dilution of a 10 mg L^{-1} mercury stock solution with DDD water. ACS reagent grade HCl, NaOH and buffer solutions (Merck, Germany) were used to adjust the solution pH to the required value.

The *Theobroma cacao* pod husks were obtained from a farm in Mbele, in the Central region of Cameroon (4°10′0.02″N and 11° 32′00″E), Africa. Primary treated municipal wastewater (MWW) samples were collected from the central municipal processing plant in Pretoria, South Africa (25.7256°S and 28.2439°E). They were filtered through Whatman paper #4 (USA) to remove suspended particles and then stored in a laboratory fridge at 4 °C until analysis within one week.

2.3. Preparation of Activated Carbon

The preparation of activated carbon was carried out according to the procedure recommended by Martinez *et al.*[23] The solid residue of *Theobroma cacao* was manually chosen, cleaned with deionized water, dried at 100 °C for 24 h, ground and passed through a sieve to obtain samples of 1–2.5 mm particle size. This raw material was treated with $ZnCl_2$ and $ZnCl_2/FeCl_3$ at two different concentrations (50 and 75 %, m/m), ($ZnCl_2$, $ZnCl_2/FeCl_3$ solution/char, m/m) and pyrolyzed in a tubular oven (Lindberg Blue), at three different temperatures (350, 450 and 550 °C). These ratios were selected from previous investigations[24] which showed that the adsorption capacity increases remarkably with increasing $ZnCl_2$/char ratio. After the activation, the excess $ZnCl_2$ and $ZnCl_2/FeCl_3$ were removed with a 0.1 M solution of hydrochloric acid (HCl), and then the product was washed with hot distilled water until a neutral pH was reached to obtain the sample for sorption measurements.

2.4. Characterization of Activated Carbons

The prepared activated carbons (ACs) from *Theobroma cacao* pod husk were examined with a scanning electron microscope (SEM) coupled to an X-ray (EDX) analyzer. N_2-physisorption experiments (adsorption isotherms for pore size distribution (PSD) and surface area) were conducted with a Micromeritics ASAP 2010 (USA) surface area and porosity analyzer. Analyses of adsorption and desorption of nitrogen were conducted at 195 °C. Before the experiments, the sample was degassed at 200 °C overnight. Total surface areas were determined by applying the BET equation.[25] External surface areas were determined by applying the t-plot model between the range 7–9 Å.[26] Pore size distributions were determined using both BJH methods.

Field emission scanning electron microscopy (FE-SEM) and energy-dispersive X-ray (EDX) analysis were conducted to observe the surface morphology of the ACs. The samples were gold coated to improve their conductivity to obtain good images. Elemental analysis (EA) for the carbon (C), nitrogen (N), oxygen (O), sulfur (S) and metal content of the various samples was carried out with the aid of the energy dispersive-X-ray device. The instrument used to obtain SEM images of the samples and EDS spectra was a JEOL JSM-7600F field emission scanning electron microscope, 800 mm^2, X-Max coupled to a silicon drift energy dispersive X-ray detector (SDD) (Oxford Instruments Ltd, UK).

2.5. Batch Adsorption Studies

The adsorbate stock solution of 1000 mg L^{-1} Hg^{2+} was prepared from HgCl2 in distilled water. This stock solution was diluted as required to obtain standard solutions containing 10–100 ng L^{-1} Hg^{2+}. Batch mode adsorption studies were carried out with 0.05 g of adsorbent and 50 mL of Hg^{2+} solution of a desired concentration in 100 mL conical flasks and were agitated at 160 rev min^{-1} for predetermined time intervals at room temperature in a mechanical shaker. The removal kinetics of Hg^{2+} were investigated by taking samples of the solution after the desired contact time (20–120 min) and the adsorbent was analyzed for its Hg^{2+} concentration with a RA–915$^+$ Zeeman mercury analyzer.

2.6. Data Treatment

2.6.1. *Isotherm Models*

The sorption equilibrium data for Hg^{2+} on activated carbons were analyzed by means of the Freundlich and Langmuir isotherm models.[27] The Freundlich isotherm equation $x/m = k_f C^{1/n}$ can be written in the linear form as given in Equation 1.

$$\log\left(\frac{x}{m}\right) = \log K_F + \frac{1}{n}\log C_e \qquad (1)$$

where x/m and C_e are the equilibrium concentrations of Hg^{2+} in the adsorbed and liquid phases in ng g^{-1}, and K_F and n are the Freundlich constants that are related to the sorption capacity and intensity, respectively. The Freundlich constants K_F and n can be calculated from the slope and intercept of the linear plot of log (x/m) against logC_e.

The Langmuir sorption isotherm equation $\frac{x}{m} = \frac{Q_{max} K_L C_e}{1 + k_L C_e}$ on linearization becomes:

$$\frac{C_e}{Q_e} = \frac{1}{K_L Q_{max}} + \frac{1}{Q_{max}} C_e \quad (2)$$

where Q_{max} is the maximum adsorption capacity (ng g^{-1}) when all adsorption sites are occupied, C_e (ng L^{-1}) is the equilibrium concentration of mercury, Q_e is the equilibrium adsorption capacity and the Langmuir constant K_L (dm^3 ng^{-1}) is derived from the ratio of the adsorption rate constant to the desorption rate constant.

2.6.2. *Kinetics Models*

Kinetics adsorption data were fitted to the pseudo-first-order kinetics model.[28]

$$\frac{dq_t}{dt} = k_1(q_e - q_t) \quad (3)$$

where q_e and q_t refer to the amount of Hg^{2+} adsorbed (ng g^{-1}) at equilibrium and at any time, t (min), respectively, and k_1 is the rate constant for pseudo-first-order sorption (min^{-1}). Integration of Equation 3 for the boundary conditions $t = 0$ to t and $q_t = 0$ to q_t, gives Equation 4:

$$\log\frac{q_e}{(q_e - q_t)} = \log q_e - \frac{k_1 t}{2.303} \quad (4)$$

Equation 4 is rearranged to give Equation 5:

$$\log(q_e - q_t) = \log q_e - \frac{k_1 t}{2.303} \quad (5)$$

The slope of a plot of $\log(q_e - q_t)$ *versus* t was used to determine the first-order rate constant, k_1. In many cases, the first-order equation of Lagergren[28] does not fit well for the whole range of contact times and is generally applicable over the initial stage of the adsorption processes.[29] Kinetics data were further treated with the pseudo-second-order kinetic model.[29] The pseudo-second-order equation is also based on the sorption capacity of the solid phase. Contrary to the other model, it predicts the behaviour over the whole range of adsorption and is in agreement with an adsorption mechanism involving the rate-controlling step. The differential equation is given by Equation 6:

$$\frac{dq_t}{dt} = k_2 (q_e - q_t)^2 \quad (6)$$

where k_2 is the rate constant for pseudo-second-order adsorption (g ng^{-1} min^{-1}). Integrating Equation 6 for the boundary conditions $t = 0$ to t and $q_t = 0$ to q_t, gives Equation 7:

$$\left(\frac{t}{q_t}\right) = \left(\frac{t}{q_e}\right) + \left[\left(\frac{1}{k_2 q_e^2}\right)\right] \quad (7)$$

This is the integrated rate law for a pseudo-second-order reaction. Equation 7 can be rearranged to obtain a linear form (Equation 8):

$$\left(\frac{t}{q_t}\right) = \left(\frac{t}{q_e}\right) + \left[\left(\frac{1}{k_2 q_e^2}\right)\right] \quad (8)$$

The slope and intercept of a plot of t/q_t *versus* t were used to calculate the second-order rate constant, k_2. This model is more likely to predict the behaviour over the whole range of adsorption and is in agreement with the chemisorption mechanism being the rate-controlling step.[30]

2.6.3. *Adsorption Mechanism*

In order to gain insight into the mechanism and rate-controlling step affecting the kinetics of adsorption, the kinetics experimental results were fitted to the Weber and Morris intra-particle diffusion model,[31] in which the rate of intra-particle diffusion is a function of $t^{1/2}$ and can be defined according to Equation 9:

$$q = f\left(\frac{D_t}{r_p^2}\right)^{1/2} = k_w t^{1/2} \quad (9)$$

where r_p is the particle radius, D_t is the effective diffusivity of solutes within the particle, and k_w is the intra-particle diffusion rate. Values of k_w can be obtained by linearizing the curve $q = f(t^{1/2})$. Such types of plots may present multi-linearity, implying that the overall adsorption process may be controlled by one or more steps, such as film or external diffusion, intra-particle diffusion and a chemical reaction on the pore surface, or a combination of more than one step. Weber and Morris[31] reported that if intra-particle diffusion was involved in the adsorption process, then a plot of the square root of time *versus* the adsorption amount would result in a linear relationship, and that the intra-particle diffusion would be the controlling step if this line passes through the origin.

3. Results and Discussion

3.1. Characterization of Activated Carbons

In this work, *Theobroma cacao* pod husk (GAC_0), an industrial effluent abundantly available from the *Theobroma* bean processing plants, was utilized as a feedstock for preparation of activated carbon (GAC8: T = 550 °C, 75 % Zn for 3 h), GAC1 (T = 450 °C, 50 % Zn for 3 h) and GAC7 (T = 550 °C, 50 % Zn/Fe for 3 h) *via* microwave-induced 50 and 75 % (w/w) of $ZnCl_2$ and $FeCl_3$ activation

3.1.1. *Surface Areas and Pore Sizes*

The N_2 adsorption isotherms at 77 K for activated carbons produced from the *Theobroma cacoa* by chemical activation are presented in Fig. 1. All the samples gave type II isotherms, characteristic of microporous materials. The adsorption isotherms show adsorption-desorption hysteresis, indicating the presence of mesopores. Besides contributing significantly to the adsorption of the adsorbate, mesopores could be attributed to the interaction of functional groups at the surface of char which favours the evolution of molecules during the heating process of activation, then probably creating external pores.[32] The overall porosity development determined by N_2 adsorption at 77 K by the BET and BJH methods are shown in Table 1. It shows that all the samples have surface areas between 357.36 and 586.93 m^2 g^{-1} with highly developed microporosity.

3.1.2. *Functionalization*

The Fourier transform infrared (FTIR) spectra of the activated carbons are shown in Fig. 2. The absorption at 2958 cm^{-1} indicates the presence of C-H groups.[33] The peaks appearing at 1542.1 and 1504.6 cm^{-1} are as a result of carbonyl groups (C=O) while

Table 1 Characteristics of the *Theobroma cacao* pod husk activated carbons.

Activated carbons	S_{BET}/m^2 g^{-1}	S_L/m^2 g^{-1}	S_{BJH}/m^2 g^{-1}	V_{TOTAL}/cm^3 g^{-1}	V_{BJH}/cm^3 g^{-1}	S_{BJH}/S_{BET}	D_{BET}/Å
GAC1	457.35	512.32	69.327	0.102	0.083	0.151	24.931
GAC7	357.36	446.76	54.235	0.109	64.678	0.152	21.068
GAC8	586.93	777.37	133.614	0.155	0.143	0.227	42.807

(n = 3 and 5 % error).

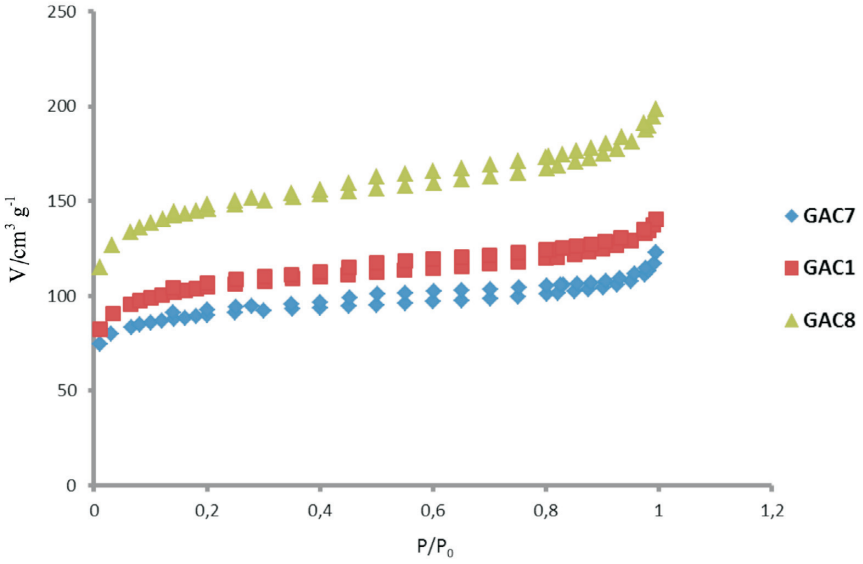

Figure 1 Nitrogen adsorption/desorption isotherms for *Theobroma cacao* pod husk ACs.

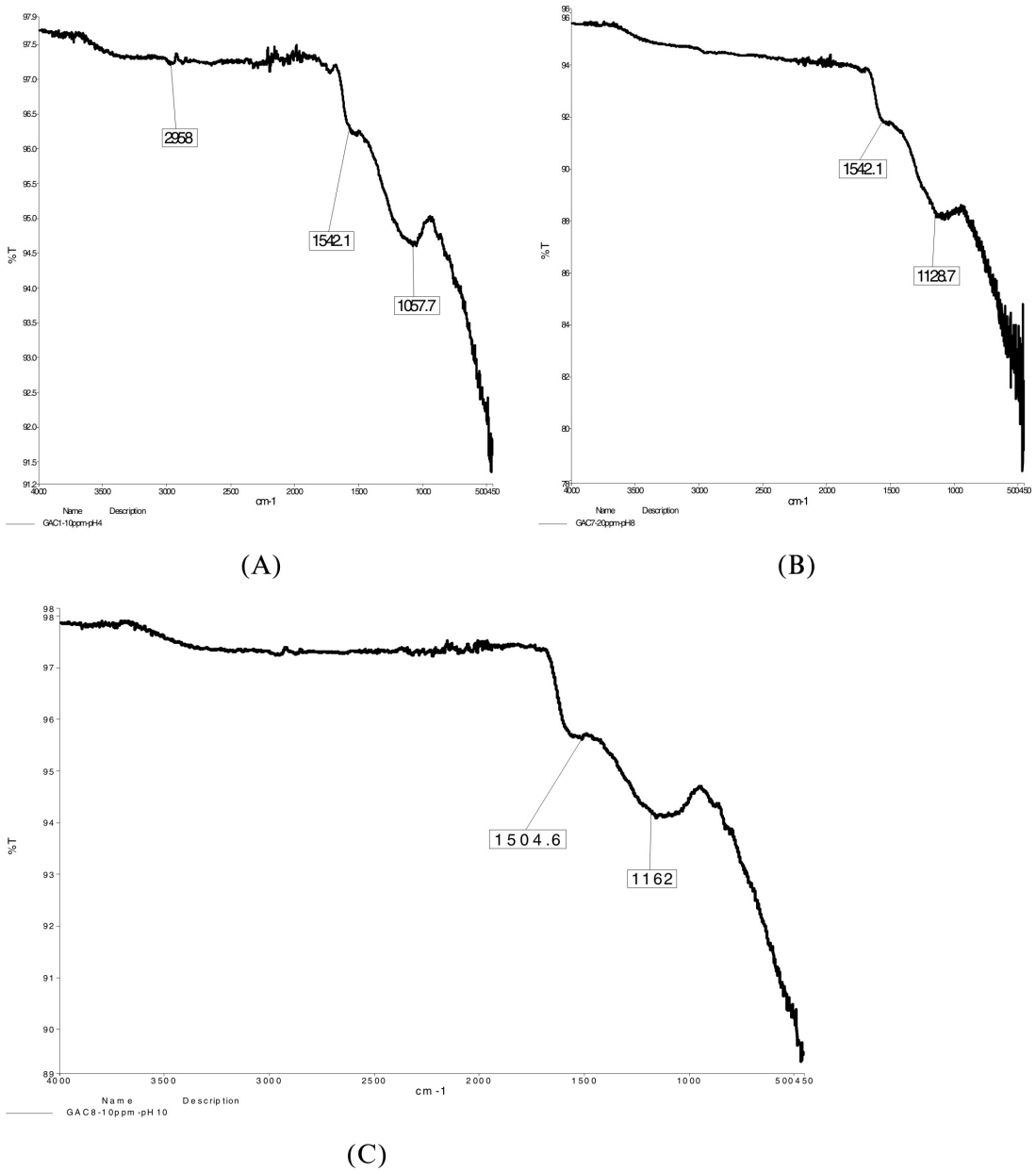

Figure 2 FTIR spectra for GAC1 (**A**), GAC7 (**B**) and GAC8 (**C**).

the bands appearing at 1057.7, 1128.7 and 1162 cm^{-1} are ascribed to the formation of sulfur functional groups like a highly conjugated S=O.

3.1.3. *Surface Morphology*

To observe the morphology of the prepared AC samples, SEM images are shown in Fig. 3. Fig. 3A shows the micrograph for *Theobroma cacao* pod husk employed as the raw material for the preparation of the activated carbons. The material presents a surface morphology in the form of plates, possibly with a low specific surface area. The micrographs shown in Fig. 3B, C, D correspond to the materials collected after the activation process with $ZnCl_2$ and $FeCl_3$, with the salt mixture of 50 % Zn, 75 % Zn and 75 % Zn/Fe, respectively, for GAC1, GAC8 and GAC7. These images show that the morphology of the samples has changed after the activation process; suggesting that surface craters were produced, which contributes to the increase of the surface area after the activation. From this analysis, it is clear that the presence of zinc and iron species in the preparation of the samples produces 'craters' with thinner walls on the surfaces, thereby creating a weaker structure.

3.2. Batch Adsorption Studies

3.2.1. *Effect of Contact Time*

Figure 4 shows the effect of contact time on the removal of Hg^{2+}. Experimental studies were carried out with varying adsorbents (GAC_1, GAC_7 and GAC_8) with 100 ng L^{-1} of the initial mercury ion concentration. Equilibrium adsorption was established within 60 min for the metal ion. These data are important because equilibrium time is one of the parameters for economical wastewater treatment plant application in agreement with other authors.[18] According to these results, the agitation time was fixed at 2 h for the rest of the batch experiments to make sure that equilibrium was attained.

3.2.2. *Effect of pH*

Figure 5 presents the effect of initial pH on the removal of Hg^{2+} by the GACs. It can be shown by speciation calculations that in the presence of Cl- the predominant species at pH > 6.0 are $Hg(OH)_2$ and $HgCl_2$, while at pH < 6.0 it is $HgCl_2$.[34] The formation of $HgCl_2$ has been found to decrease the Hg^{2+} sorption onto a commercial FS-400 GAC.[18] Accordingly, the adsorption of

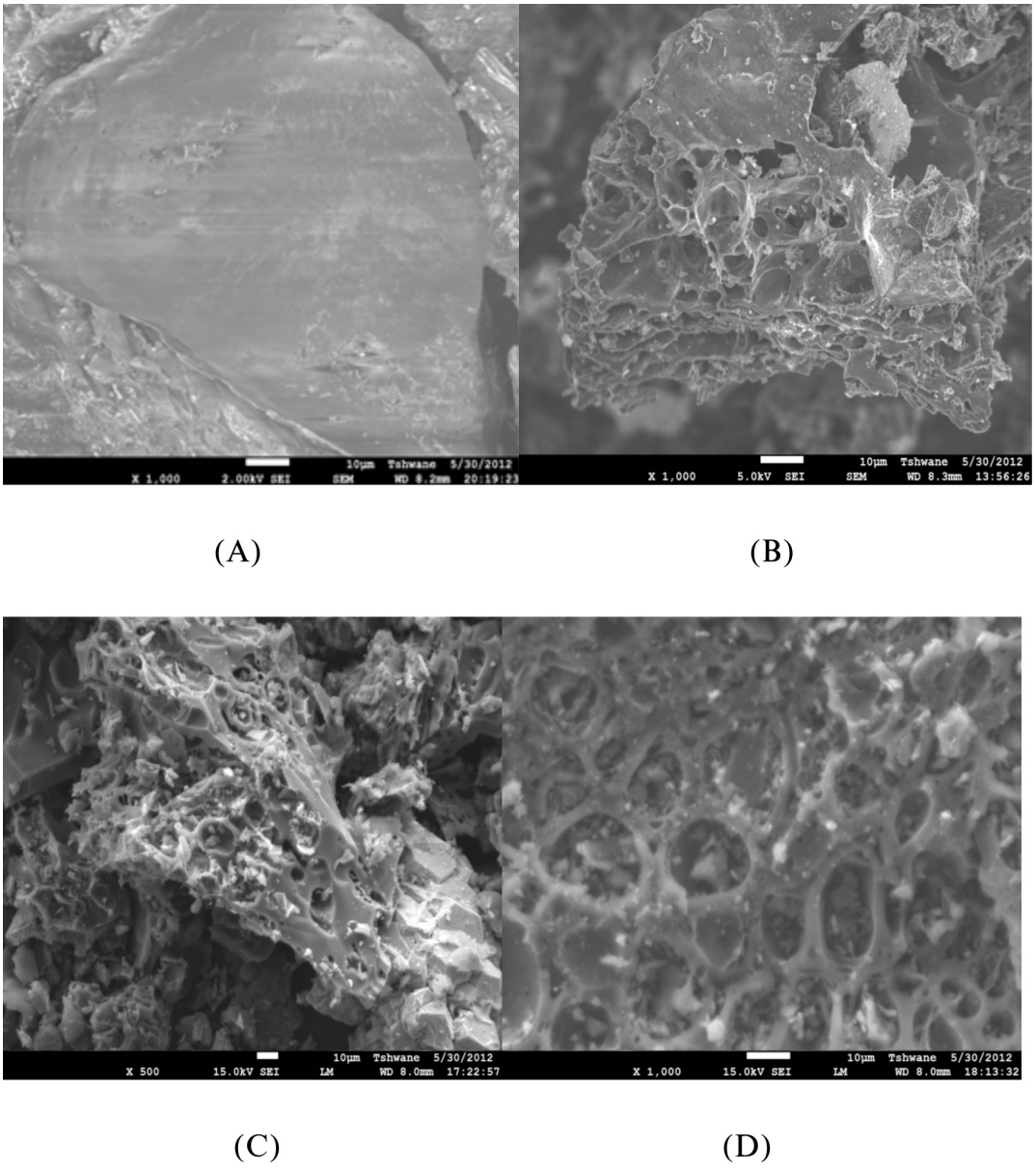

Figure 3 SEM images of GAC_0 (**A**), GAC1 (**B**), GAC7 (**C**) and GAC8 (**D**).

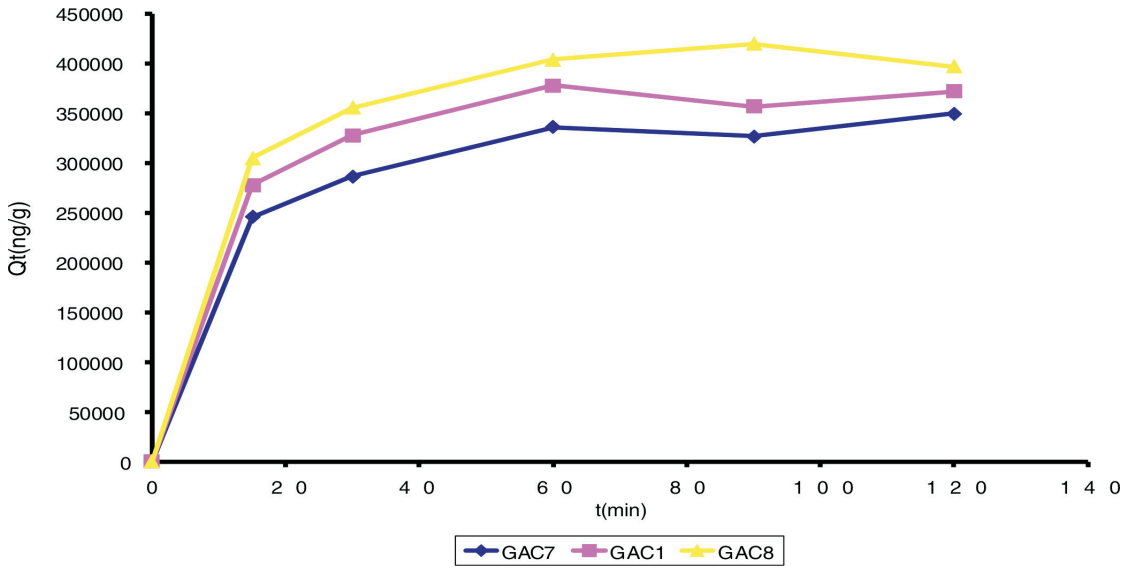

Figure 4 Effect of agitation time on the adsorption of Hg(II) for GACs. Conditions: carbon concentration, 50 mg 50 mL^{-1} (n = 3 and 5 % error).

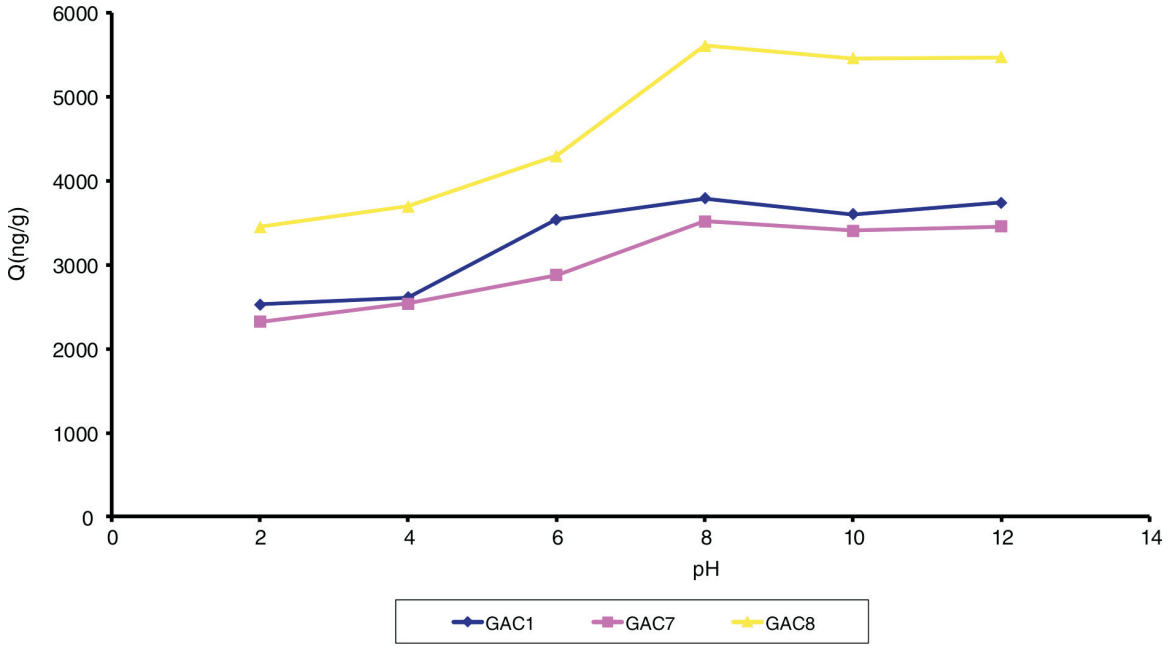

Figure 5 Effect of pH on Hg^{2+} removal. Conditions: agitation time, 2 h; carbon concentration, 50 mg 50 mL^{-1}; initial concentration, 50 ng L^{-1} (n = 3 and 5 % error).

Hg(II) decreased when the pH was lowered from 7.0 to 2.0. On increasing the pH from 6, the adsorption capacity increased and became constant over the pH range of 8.0–12.0. This implies that $Hg(OH)_2$ species may be retained in the micropores of carbon particles by chemisorption involving surface complexes.[18] Functional groups, such as $CxOH^+$, are assumed to be present on the surface of the carbons. When Hg^{2+} is present in the solution, the following surface complexes may be formed:

$$2CxOH^+ + Hg^{2+} \rightarrow (CxO)_2Hg^{2+} + 2H^+ \quad (10)$$

$$2CxONa^+ + Hg^{2+} \rightarrow (CxO)_2Hg^{2+} + 2Na^+ \quad (11)$$

3.2.3. *Equilibrium Isotherms*

Adsorption isotherms provide information on the nature of the solute-surface interaction as well as the specific relation between the concentration of adsorbate and its degree of accumulation onto the adsorbent surface at constant temperature. These equilibrium experiments were performed at room temperature with an adsorbent mass of 0.05 g and an adsorbate concentration (C_0) ranging from 25–125 ng L^{-1}. In order to understand the adsorption mechanism of mercury onto activated carbon, two adsorption isotherm models, Langmuir and Freundlich, were used to fit the experimental data. The isotherm parameters were determined by non-linear regression with Origin version 7.0, a Microsoft Windows-based statistical software. The adsorption isotherms obtained for the various GACs are illustrated in Fig. 6A and Fig. 6B. The values of the parameters and the correlation coefficients obtained for the different adsorbents are listed in Table 2. It is well known that the Langmuir model is usually used with an ideal assumption of a monolayer adsorption surface.[27] The value of the correlation coefficients (R^2) for the two models for different GACs show that the best fit was obtained with the Langmuir model. The essential characteristics of the Langmuir isotherm can be expressed in terms of a dimensionless constant separation factor or equilibrium parameter, R_L, which is defined as $R_L = \frac{1}{1 + K_L C_0}$ where K_L is

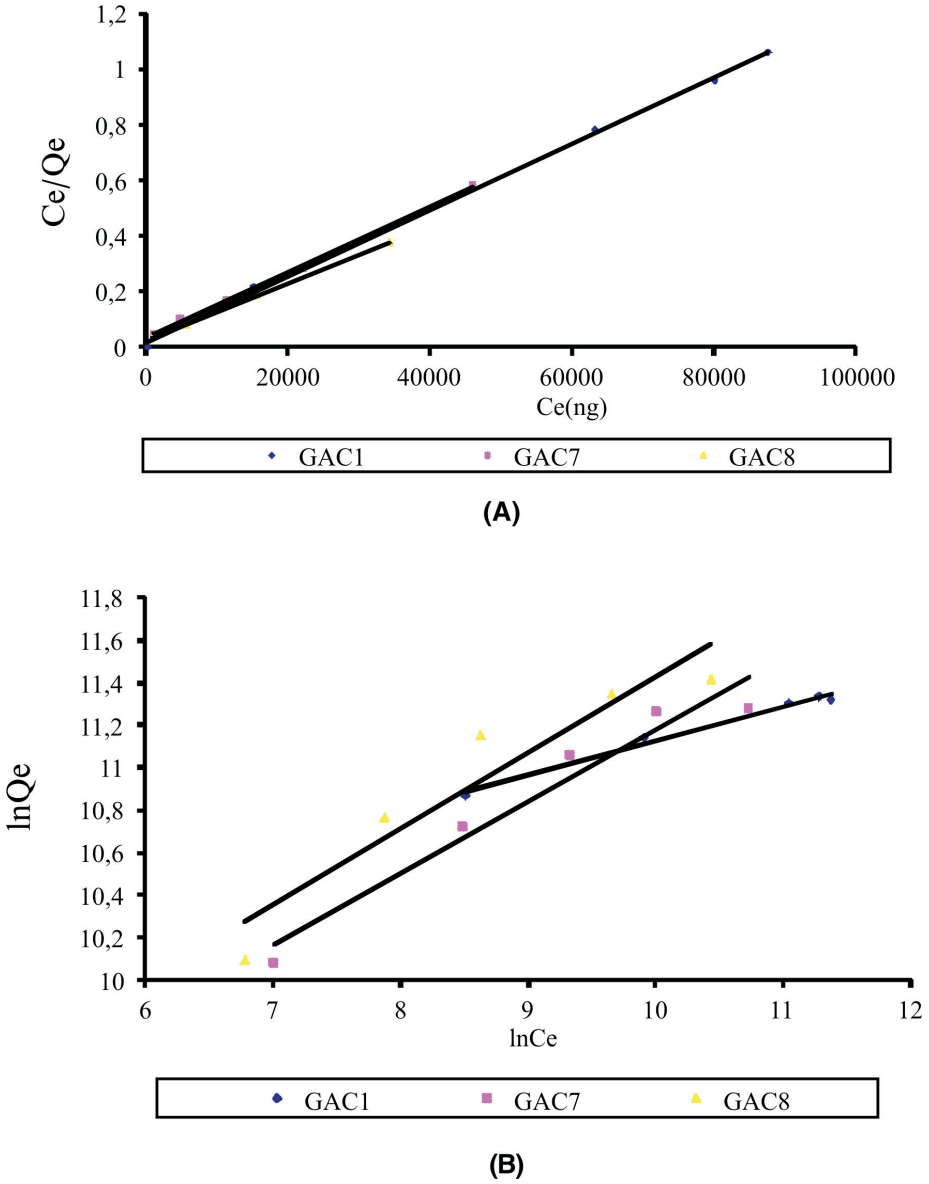

Figure 6 Langmuir (**A**) and Freundlich (**B**) isotherms for mercury adsorption onto GACs at room temperature (n = 3 and 5 % error).

the Langmuir constant and C_0 is the initial concentration of Hg^{2+}. The R_L value indicates the shape of the isotherm as follows: $R_L > 1$, unfavourable; $R_L = 1$, linear; $0 < R_L < 1$, favourable; and $R_L = 0$, irreversible. According to Mckay *et al.*,[29] R_L values between 0 and 1 indicate favourable adsorption. The R_L values for Hg^{2+} were 0.019, 0.038 and 0.026 for GAC1, GAC7 and GAC8, respectively, for 100 ng L^{-1}. Hence, the adsorption of the Hg^{2+} on GACs seems to be favourable.

Table 2 Isotherm parameters for mercury adsorption onto GAC1, GAC7 and GAC8.

Langmuir	GAC1	GAC7	GAC8
Q_{max}/ng g^{-1}	10^5	10^5	10^5
K_L/L ng^{-1}	0.0005	0.00025	0.00037
R^2	0.998	0.997	0.999
R_L	0.019	0.038	0.026
Freundlich			
K_f/ng g^{-1}	13545.369	2423.577	2540.458
n	6.218	2.952	2,787
R^2	0.968	0.948	0.902

3.2.4. *Kinetics Studies*

In order to investigate the kinetics of adsorption of mercury, the Lagergren-first-order model[28] and Ho's pseudo-second-order model[30] were used. The values of the parameters and the correlation coefficients obtained by using non-linear regression with Origin version 7.0 at room temperatures are listed in Table 3. The fit of the experimental data to the kinetics models is illustrated in Fig. 7. It was found that Ho's pseudo-second-order model gave the highest values of the correlation coefficients and predicted q_e more accurately than the other model investigated. Therefore, Ho's pseudo-second-order model could be used for the prediction of the kinetics of adsorption of mercury on the activated carbon.

3.2.5. *Adsorption Mechanism*

Figure 8 shows the intra-particle diffusion plot for the adsorption of mercury on the three activated carbons (GAC1, GAC7 and GAC8). From Fig. 8, it can be seen that the plots for GAC1, GAC7 and GAC8 show similar features; they have one linear segment followed by a plateau. In the first 60 min, the first linear portion did not pass through the origin, implying that the intra-particle diffusion did not play an important role and did not control the

Table 3 Kinetics parameters for mercury adsorption onto *Theobroma cacao* pod husk activated carbons.

Model	Lagergren		Pseudo second order			Intra-particle diffusion		
	K_1/min^{-1}	R^2	K_{2app}/g ng^{-1} min^{-1}	R^2	h/ng g^{-1} min^{-1}	K_w/ng g^{-1} min$^{-0.5}$	R^2	I
GAC1	0.053	0.832	4.5×10^{-7}	0.997	10^4	13829	0.874	205020
GAC7	0.061	0.887	9×10^{-8}	0.987	10^4	12123	0.727	251550
GAC8	0.042	0.930	4×10^{-8}	0.995	5×10^4	13974	0.756	271414

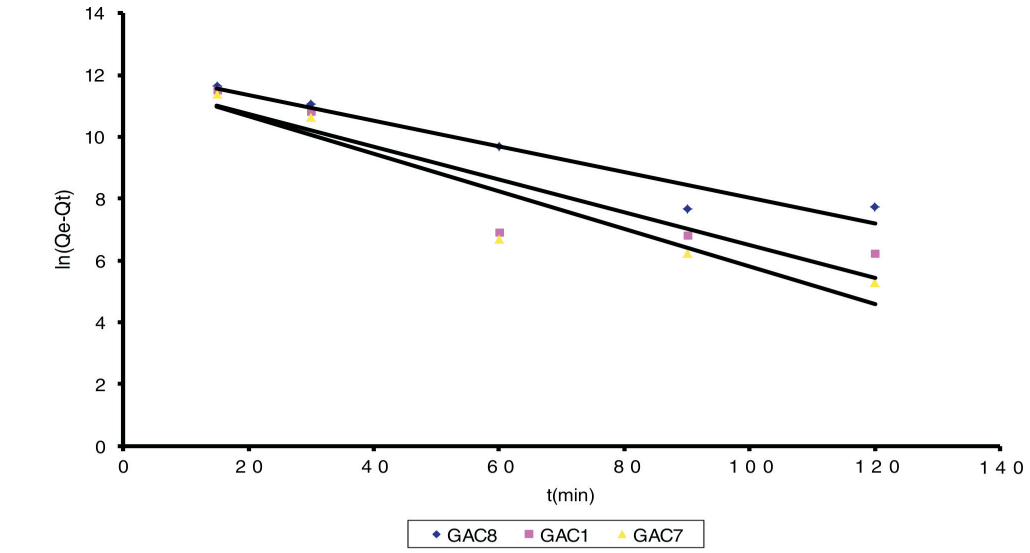

(A)

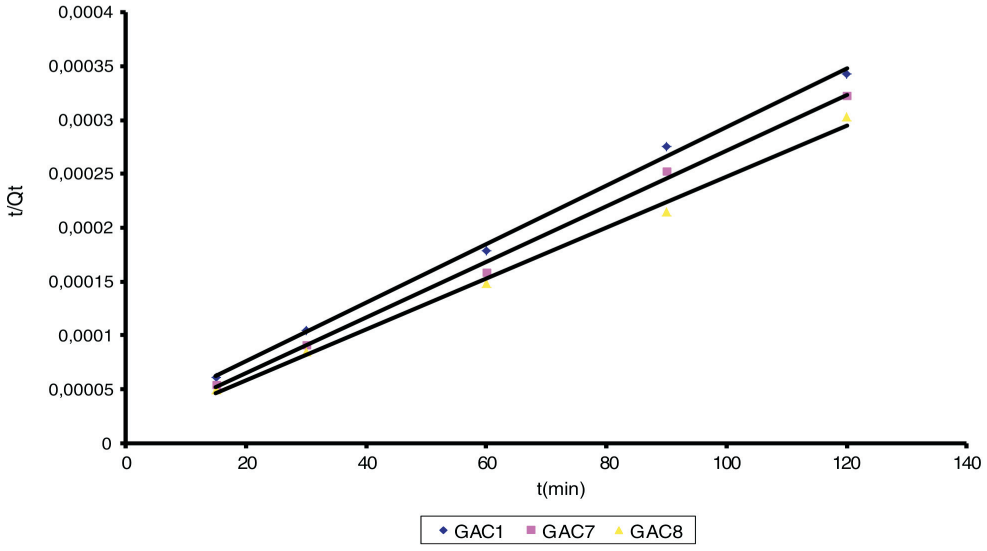

(B)

Figure 7 Fit of the pseudo-first-order (**A**) and pseudo-second-order (**B**) kinetics models for the adsorption of Hg^{2+} onto GACs for C_0 = 100 ng L^{-1} (n = 3 and 5 % error).

rate of the adsorption. After 60 min, the regression was nearly linear but did not pass through the origin, suggesting that intra-particle diffusion was not the sole rate-controlling step in this stage. The k_w value evaluated from the first linear parts of these curves for GAC1, GAC7 and GAC8 were 13829, 12123 and 13974 (ng g^{-1} min$^{-0.5}$), respectively. The k_w value increased with increasing impregnation of $ZnCl_2$, which showed that the adsorption rate increased with increasing impregnation of $ZnCl_2$. Comparing plots of GAC1, GAC7 and GAC8, the plot of GAC8 had an added curved portion in the first 60 min, showing that film diffusion played an important pole in this stage.[31]

4. Conclusions

The present investigation shows that the *Theobroma cacao* activated carbon was an effective and low-cost adsorbent for the removal of mercury(II) from dilute aqueous solution. The surface areas of the prepared activated carbons were relatively high with large pore volumes and were found to be microporous. The maximum adsorption capacity of mercury was found to be 10^5 ng g^{-1} for GACs for an initial mercury concentration of 100 ng L^{-1}. The Langmuir and Freundlich isotherm equations were used to interpret the adsorption phenomenon of the adsorbate. The Langmuir isotherm was found to best describe the

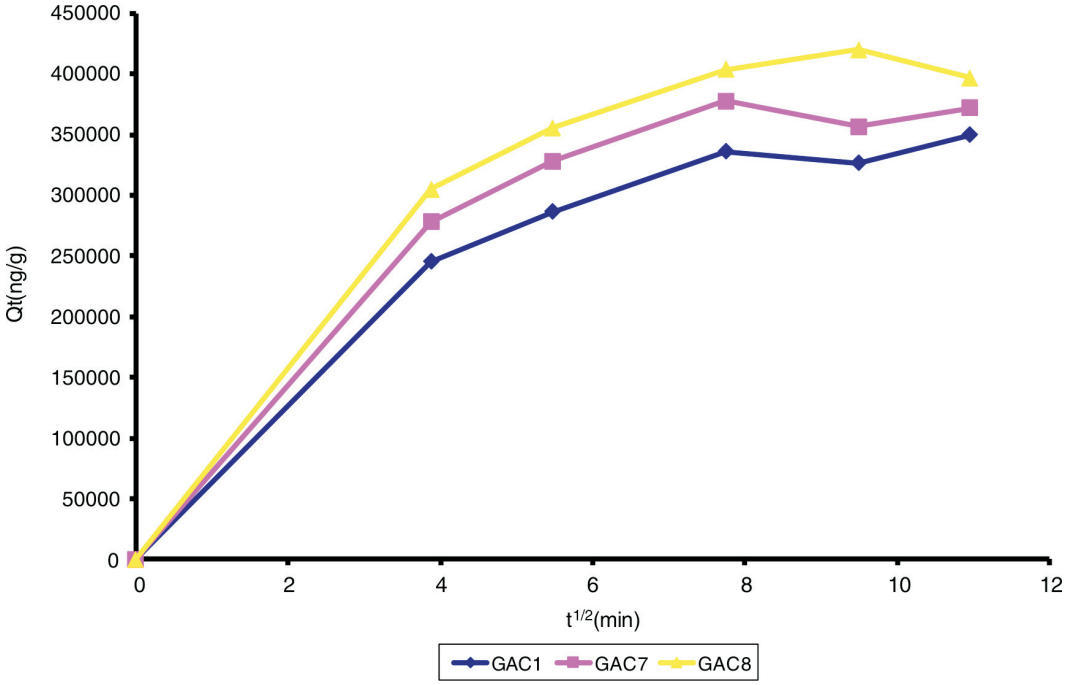

Figure 8 Plot of the intra-particle diffusion model for the adsorption of Hg^{2+} on GACs for C_0 = 100 ng L^{-1} (n = 3 and 5 % error).

experimental data. The kinetics of adsorption was modelled with the Lagergren-first-order and pseudo-second-order equations, and the pseudo-second-order equation was found to explain the adsorption kinetics most effectively. Carbonyl and sulfur functional groups present on the surface of the adsorbents were involved in chemical interaction with mercury as revealed from the FTIR spectra. It was also found that pore diffusion played an important role in the adsorption.

Acknowledgements

This research was supported by the Universities of Yaoundé I and Douala, both in Cameroon. Appreciation is expressed to the Academy of Sciences for the Developing World (TWAS) in Trieste, Italy, for financial assistance to the main author to travel to the host institution, the Tshwane University of Technology (TUT), in Pretoria, South Africa, working under Profs R.I. McCrindle and P.P. Ndibewu. Finally, the National Research Foundation (NRF) of South Africa is thanked for having provided funds to the host institution (TUT) necessary for the procurement of chemicals used throughout the entire project.

References

1 E.G. Pacyna, J.M. Pacyna, J. Fudala, J.E. Strzelecka, S. Hlawicska and D. Panasiuk, Mercury emissions to the atmosphere from anthropogenic sources in Europe in 2000 and their scenarios until 2020, *Sci. Total Environ.*, 2006, **370**, 147–156.

2 A. Kirby, I. Rucevska, V. Yemelin, C. Cooke, O. Simonett, V. Novikov and G. Hughes, *UNEP Global Mercury Assessment: Sources, Emissions, Releases and Environmental Transport*, United Nations Environment Protection (UNEP), Report, 2013.

3 http://www.unep.org/PDF/PressReleases/GlobalMercuryAssessment 2013.pdf [accessed 19 August 2013].

4 A. Bhan and N.N. Sarkar, Mercury in the environment: effect on health and reproduction, *Rev. Environ. Health*, 2005, **20**, 39–43.

5 J.C. Clifton II, Mercury exposure and public health, *Pediatr. Clin. North Am.*, 2007, **54**, 237–245.

6 U.S. EPA (U.S. Environmental Protection Agency). http://www.epa.gov/mercury/ [accessed 10 October 2013].

7 M.H.G. Berntssen, A. Aatland and R. D. Handy, Chronic dietary mercury exposure causes oxidative stress, brain lesions, and altered behaviour in Atlantic salmon (*Salmo salar*) parr, *Aquatic Toxicol.*, 2003, **65**, 55–72.

6 WHO, *Environmental Health Criteria 118, Inorganic Mercury*, World Health Organization, Geneva, 1991, pp. 68–112.

9 J.H. Cai and C.Q. Jia, Mercury removal from aqueous solution using coke-derived sulfur-impregnated activated carbons, *Ind. Eng. Chem. Res.*, 2010, **49**, 2716–2721.

10 T. Viraraghavan and A. Kapoor, Adsorption of mercury from wastewater by bentonite, *Appl. Clay Sci.*, 1994, **9**, 31–49.

11 S. Kushwaha, G. Sreelatha and P. Padmaja, Physical and chemical modified forms of palm shell: preparation, characterization and preliminary assessment as adsorbents, *J. Porous. Mater.*, 2013, **20**, 21–36.

12 M. Eloussaief, A. Sdiri and M. Benzina, Modelling the adsorption of mercury onto natural and aluminium pillared clays, *Environ. Sci. Pollut. Res.*, 2013, **20**, 469–479.

13 A. Bhatnagara and M. Sillanpää, Utilization of agro-industrial and municipal waste materials as potential adsorbents for water treatment: a review, *Chem. Eng. J.*, 2010, **157**, 277–296.

14 A. Azizah, N. Nikruslawati and T.T. Swee, Extraction and characterization of antioxidant from cocoa by-products, *Food Chem.*, 1999, **64**, 199–202.

15 R. Redgwell, V. Trovato, S. Merinat, D. Curti and S. Hediger, Dietary fibre in cocoa shell: characterisation of component polysaccharides, *Food Chem.*, 2003, **81**, 103–112.

16 E. Aregheore, Chemical evaluation and digestibility of cocoa (*Theobroma cacao*) by products fed to goats, *Trop Anim. Health Pro.*, 2002, **34**, 339–348.

17 A. Oladayo, Proximate composition of some agricultural wastes in Nigeria and their potential use in activated carbon production, *J. Appl. Sci. Environ. Manag.*, 2010, **14**, 55–58.

18 A. Basu, M.S. Rahaman, S. Mustafiz and M.R. Islam. Batch studies of lead adsorption from a multi-component aqueous solution onto Atlantic cod fish scale (*Gadus morhua*), *J. Environ. Eng. Sci.*, 2007, **6**, 455–462.

19 K. Kadirvelu, M. Kavipriya, C. Karthika, M. Radhika, N. Vennilamani and S. Pattabhi, Utilization of various agricultural wastes for activated carbon preparation and application for the removal of dyes and metal ions from aqueous solutions, *Bioresource Technol.*, 2003, **87**, 129–132.

20 C. Bin, W. Xiaoru and F.S.C. Lee, Pyrolysis coupled with atomic absorption spectrometry for the determination of mercury in Chinese medicinal materials, *Anal. Chim. Acta.*, 2001, **447**, 161–169.

21 N. Panichev, M.M. Kalumba and K.L. Mandiwana, Solid phase

extraction of trace amount of mercury from natural waters on silver and gold nanoparticles, *Anal. Chim. Acta.*, 2014, **813**, 56–62.

22 N.A. Panichev, Panichev and S.E. Panicheva, Determination of total mercury in fish and sea products by direct thermal decomposition atomic absorption spectrometry, *Food Chem.*, 2015, **166**, 432–441.

23 S. Sholupov, S. Pogarev, V. Ryzhov, N. Moshynov and A. Stroganov, Zeeman atomic absorption spectrometer RA-915+ for direct determination of mercury in air and complex matrix samples. *Fuel Process Technol.*, 2004, **85**, 473–485.

24 M.L. Martinez, M.M. Torres, C.A. Guzman and D.M. Maestri, Preparation and characteristics of activated carbon from olive stones and walnut shells, *Indust. Crops Products*, 2006, **23**, 23–28.

25 L.C.A. Oliveira, E. Pereiraa, I. R. Guimaraesa, A. Valloneb, M. Pereirac, J. P. Mesquitac and K. Sapag, Preparation of activated carbons from coffee husks utilizing $FeCl_3$ and $ZnCl_2$ as activating agents, *J. Hazard Mater.*, 2009, **165**, 87–94.

26 C.O. Ania, B. Cabal, J.B. Parra and J.J. Pis, Importance of hydrophobic character of activated carbons on the removal of naphthalene from the aqueous phase, *Adsorp. Sci.*, 2007.

27 B.C. Lippens, & J.H. Deboer, Studies on pore systems in catalysts V. The t-plot method. *J. catal.*, 1965, **4**, 319–323.

28 C.M. Kede, M.A. Etoh, P.P. Ndibewu, H.M. Ngomo and P.M. Ghogomu, Equilibria and kinetic studies on the adsorption of cadmium onto Cameroonian wetland clays. *British J. Applied Sci. Technol.*, 2014, **4**(7), 1070–1088.

29 S. Lagergren, About the theory of so-called adsorption of soluble substances, *Kungl. Svenska vetakad. handl.*, 1898, **24**, 1–39.

30 Y.S. Ho and G. McKay, The sorption of Lead(II) on peat, *Water Res.*, 1999, **33**, 578–584.

31 Y.S. Ho and G. McKay, Pseudo-second order model for sorption processes, *Process Biochem.*, 1999, **34**, 451–465.

32 W.J. Weber and J.C. Morris, Kinetics of adsorption on carbon from solution, *J. Sanitary Eng. Div. Proceed. Am. Soc. Civil. Eng.*, 1963, **89**, 31–59.

33 R.N. Abdoul, B.B. Loura, B. Abdelaziz and J.M. Ketcha, Modified composite activated carbon derived from post-consumer plastics and lignocellulosic materials; *Amer. Chem. Sci. J.*, 2013, **3**(1), 24–33.

34 G. Socrates, *Infrared and Raman Characteristic Group Frequencies: Tables and Charts*, 3rd edn., John Wiley & Sons, West Sussex, United Kingdom, 2001.

34 D. Mohan, V.K. Gupta, S.K. Srivastava and S. Chander, Kinetics of mercury adsorption from wastewater using activated carbon derived from fertilizer waste, *Colloids Surfaces A: Physicochem. Eng. Aspects,* 2001, **177**, 169–181.